Chemical Engineering Journal 459 (2023) 141596

Contents lists available at ScienceDirect

Chemical Engineering Journal

journal homepage: www.elsevier.com/locate/cej

A general Metal-Ion-Modification route for preparing hydrophobic paper and tableware from lignocellulose fibers

R.M. Oshani Nayanathara [a], Weiqi Leng [b], Senal D. Liyanage [c], Xiang Wang [d], Lu Wang [e], Jinwu Wang [f], Zhenhua Tian [g], Charles U. Pittman Jr. [c], Steven R. Gwaltney [c], Xuefeng Zhang [a,*]

[a] Department of Sustainable Bioproducts, Mississippi State University, Mississippi State, MS 39762, USA
[b] Jiangsu Co-Innovation Center of Efficient Processing and Utilization of Forest Resources, Nanjing Forestry University, Nanjing, Jiangsu 210037, China
[c] Department of Chemistry, Mississippi State University, Mississippi State, MS 39762, USA
[d] Department of Chemistry, Zhejiang University, Hangzhou, Zhejiang, China
[e] Advanced Structures and Composites Center, University of Maine, 35 Flagstaff Road, Orono, ME 04469, USA
[f] Forest Products Laboratory, U.S. Forest Service, 1 Gifford Pinchot Drive, Madison, WI 53726, USA
[g] Department of Mechanical Engineering, Virginia Polytechnic Institute and State University, Blacksburg, VA 24061, USA

ARTICLE INFO

Keywords:
Lignocellulose fibers
Metal-ion-modification
Hydrophobization
Water-resistant
Paper tableware

ABSTRACT

Inherent hydrophilicity and poor water resistance prevent using lignocellulosic materials as green plastic alternatives to fossil fuel-based plastics. Here, we report a facile metal-ion-modification (MIM) route, swelling with aqueous metal ion solutions, and drying to convert conventional hydrophilic paper and wood pulp into biodegradable hydrophobic paper and tableware without the addition of hydrophobic sizing chemicals/materials. Metal ions such as Fe^{3+} and Zr^{4+} can coordinate with pulp fibers' polar groups (i.e., OH, C═O, and COOH) that induce self-assembly of their surface fibrillated "hairy" cellulose nanofibrils to form a more compact structure with fewer available OH groups for water sorption. This decreases the surface energy of pulp fibers and increases their hydrophobicity and water resistance. Only ~3 mg of metal ions is needed to induce the wettability transition in 1 g of kraft pulp, resulting in hydrophobic paper and tableware with water contact angles (WCAs) of 120–140°. The coordinated Fe^{3+} and Zr^{4+} are stable, with negligible metal leaching during use, allowing the hydrophobic paper and tableware to be used for food packaging. This MIM technique can be integrated into the existing paper-making process for the scalable production of hydrophobic papers and tableware, providing an alternative route for developing sustainable and biodegradable plastic counterparts.

1. Introduction

Plastic pollution is a severe global environmental issue that endangers the biosphere because accumulated plastic debris is ubiquitous and resistant to biodegradation [1]. The development of biodegradable plastics and plastic alternatives is a crucial solution for preventing the increase of plastic waste. Lignocellulose fiber-based products, including paper, molded pulp tableware [2], and casting film [3], consist of overlapping lignocellulose fibers. They are promising plastic alternatives. In 2020, global production volumes of packaging paper, paperboard, and molded pulp products amounted to 249 million tons [4]. However, the poor water resistance and low wet strength of those fiber-based products limit their potential as green plastic alternatives to fossil fuel-based plastics.

Lignocellulose fibers, including wood fibers and (un)bleached pulps, are made of cellulose microfibrils reinforced by amorphous hemicellulose and lignin macromolecules [5]. Cellulose microfibrils and their hemicellulose surface wrappings consist of abundant accessible hydroxyl groups (OHs) [6], which endow lignocellulose fibers with hydrophilic character. During the wood pulping and refining processes, microfibrils are fibrillated from the fibers upon partial removal of hemicellulose and lignin and become "hairy" nanofibrils with one end attached to the fiber's surface. These fibrillated structures have higher surface area and far more exposed OHs [7–9]. These render unsized paper and molded pulp products highly susceptible to liquid water wetting and penetration.

Extensive efforts have focused on making lignocellulose hydrophobic by physically or chemically blocking lignocellulose's surface OHs

* Corresponding author.
E-mail address: xz210@msstate.edu (X. Zhang).

https://doi.org/10.1016/j.cej.2023.141596
Received 16 December 2022; Received in revised form 24 January 2023; Accepted 26 January 2023
Available online 31 January 2023

[10–12] so that lignocellulose fiber-based products can resist water. Internal sizing using alkyl ketene dimer (AKD) and alkenyl succinic anhydride (ASA) is widely used in paper industries [11]. The AKD and ASA graft to lignocellulose's OHs through covalent bonding, resulting in an outward orientation of their long alkyl tails, thereby providing water resistance [13]. Similarly, silylation also creates a lignocellulose hydrophobic surface due to the consumption of OHs *via* covalent bonding, which covers the surface with hydrophobic polysiloxane chains. Surface deposition of inorganic nanoparticles (e.g., TiO_2, SiO_2, and Al_2O_3) *via* dip or vacuum coating can create a barrier for liquid water penetration, improving lignocellulosic fibers' water resistance [14]. Per- and polyfluorinated substances (PFAS) coatings that graft to lignocellulose's OHs impart packaging paper and tableware with good water and oil resistance [12]. In addition to the inherent limitations of these processes (e.g., AKD and ASA suffer low shelf life [10], nanoparticle deposition requires expensive precursors, PFAS leaking threatens food safety and human health [15]), the existence of lignocellulose fiber-based hydrophobization routes all rely on the addition of new hydrophobic chemicals/materials. Moreover, these hydrophobic paper-based products suffer recycling issues because they use hydrophobic additives during manufacturing [13,16]. Therefore, developing hydrophobic additive-free techniques to produce hydrophobic paper and tableware is desirable.

Water resistance of lignocellulose fibers arises from the elimination of their surface exposed/accessible OHs, which is also affected by their microstructure [6,17]. For example, all-lignocellulose fiber-based paper straw has no water resistance, while cellulose nanofiber (CNF)-reinforced lignocellulose fiber-based paper straw exhibits improved water resistance. This occurs despite the fact that CNF contains more surface-exposed OHs than lignocellulose fiber [18]. Therefore, the improved water resistance can be attributed to the denser and more compact microstructure of CNF-reinforced paper straw, which limits water penetration and absorption through capillary diffusion [6,17]. Another example is hornification, an irreversible microstructure change (i.e., pore closure) within lignocellulose fiber which results from the microfibril reorganization during drying [19]. This decreases the swelling ability of wood pulps or paper and slightly increases their water resistance [6,20]. Therefore, microstructure engineering of lignocellulose fiber could be a potential method for producing water-resistance fiber-based products without using hydrophobic additives.

Recently, multivalent metal ions (M^{x+}), including Ca^{2+}, Al^{3+}, and Fe^{3+}, have been used to assemble lignocellulose nanofibers from their water suspensions [21–24]. The positively charged M^{x+} can interact with negatively charged oxygen-containing groups (e.g., OH, C═O, and COOH) of lignocellulose nanofibers *via* coordination and/or ionic bonding [22,25]. The subsequent water evaporation step induces strong capillary force among nanofibers, inducing the crosslinking between M^{x+} and nanofibers [6] and resulting in denser films [22,24]. M^{x+}-crosslinked films exhibit better water resistance than non-crosslinked films because of their denser microstructure. Nevertheless, most of the M^{x+}-crosslinked films remain hydrophilic and cannot be used to fabricate products that require long-term water contact, such as tableware. Moreover, lignocellulose nanofibers are costly, and their production capacity is low, which cannot satisfy the increasing demand of the global sustainable packaging market.

We have now developed a novel and effective metal-ion-modification (MIM) route for converting lignocellulose fibers to hydrophobic and water-resistant paper and tableware without adding hydrophobic sizing chemicals or materials. In the MIM, conventional hydrophilic lignocellulosic paper and pulps are swelled with a dilute metal ion M^{x+} (e.g., Fe^{3+}) solution through immersion or spray, followed by water removal by drying (e.g., air drying). We took advantage of the strong multiple coordination interactions between M^{x+} and surface polar groups of lignocellulose fibers (i.e., OH, C═O, COOH). These induced the reorganization of their surface fibrillated nanofibrils to form a more compact structure with fewer available OHs to water solvation (Fig. 1**a**). This decreases pulp fibers' surface energy and increases their hydrophobicity and water resistance. The resulting hydrophobic paper exhibits comparable water resistance to synthetic polymer films *but remains biodegradable*. Moreover, the low M^{x+} content (e.g., as low as 3 mg M^{x+}/g pulp) and high M^{x+} complex stabilities allow the hydrophobic paper and tableware to be used for food packaging. This simple approach can be integrated into the existing paper-making process for scalable production of sustainable hydrophobic fibers, papers, and tableware, which could diminish the environmental impact of wide-ranging packaging applications.

2. Experimental procedures

2.1. Materials

Newspaper and cardboard were collected from local stores. Different types of papers, including A4 copy paper (Georgia-Pacific Standard Paper), Kraft packaging paper (KPP, Boardwalk K3650612), Kraft tissue paper (KTP, Tork 7171300), and conventional writing paper (WP, TOPS The Legal Pad 7572), were purchased from Amazon.com. The photographs of all tested papers are shown in Figure S1. Nanocellulose was obtained from the Process Development Center at the University of Maine (Orono, ME, USA) and was initially produced by a cellulose mechanical defibrillation process. Xylan was purchased from Sigma-Aldrich Chemical Co. (St. Louis, MO, USA). Softwood kraft lignin was obtained from Ingevity. Other chemicals, including zirconyl (IV) chloride octahydrate ($ZrOCl_2{\cdot}8H_2O$, ≥98 %), iron (III) chloride nonahydrate ($FeCl_3{\cdot}9H_2O$, ≥99 %), aluminum (III) chloride nonahydrate ($AlCl_3{\cdot}9H_2O$, ≥99 %), iron(II) chloride ($FeCl_2$), zinc (II) chloride hexahydrate ($ZnCl_2{\cdot}6H_2O$, ≥99 %), yttrium (III) nitrate [$Y(NO_3)_3$], cobalt (II) nitrate [$Co(NO_3)_2$], lithium (I) chloride (LiCl), sodium (I) chloride (NaCl), magnesium (II) chloride ($MgCl_2$), calcium (II) chloride ($CaCl_2$), methanol, ethanol, isopropanol, toluene, and hexane, were purchased from Thermo Fisher Scientific Inc. (Waltham, MA, USA).

2.2. MIM process

In a typical process, three pieces of paper (4 × 4 cm^2) were immersed in 100 mL of 60 mM metal salt solution. After a set immersion period, the paper samples were removed from the solution and rinsed with deionized water to remove the uncomplexed metal ions on the paper surface. Then, the modified papers were dried in an oven at a set temperature (60 °C for 2 h). The ions Li^+, Na^+, Mg^{2+}, Ca^{2+}, Zn^{2+}, Cu^{2+}, Co^{2+}, Fe^{2+}, Al^{3+}, Y^{3+}, Fe^{3+}, and Zr^{4+} were tested. Immersion times between 1 s and 4 h were employed, and metal ion concentrations from 0.1 mM to 1 M were studied. Drying temperatures of 25, 60, 80, and 100 °C were tested for Zr^{4+} and Fe^{3+} modified papers, and drying times ranged from 2 h to 24 h depending on the temperature. Paper samples used for mechanical testing and paper bag fabrication were performed using large-sized paper samples and large metal ion solution volumes.

Paper pulp feedstocks were employed to test the applicability of metal ion modification on pulp fiber's wettability transition. Before modification, wet pulps (200 g/L) were prepared by dispersing 20 g of kraft packaging paper into 100 mL of distilled water. The suspension was vigorously blended at 11000 rpm for 2–4 min and wet pulps were isolated by filtration. Wet pulp was modified by adding 4 g into 100 mL of aqueous 60 mM $ZrOCl_2$ or $FeCl_3$ solution and holding for 4 h. Then, the modified pulp was separated from the metal ion solution by vacuum filtration to yield a pulp sheet. The pulp sheet was rinsed with excess distilled water to remove the uncomplexed surface metal ions, followed by oven drying at 60 °C for 2 h to give the dried modified pulp sheet.

Paper lignocellulosic model compounds were modified using approximately 400 mg of nanocellulose, kraft lignin, or xylan. These compounds were dispersed into 200 mL of 60 mM aqueous $ZrOCl_2$ or $FeCl_3$ solutions for 4 h with magnetic stirring. Then, the modified model components were filtered and washed with 200 mL of deionized water

via vacuum filtration (the pore size of the filter paper was 20–25 μm). The collected filtrates were vacuum-dried at 80 °C for 2 h.

For comparison purposes, KPP, KTP, A4 paper, and pulps were also immersed in deionized water or 20–100 mM HCl solutions for 4 h, followed by oven drying at 60 °C for 2 h.

2.3. Characterizations and measurements

Water contact angles (WCAs) of conventional paper, modified hydrophobic paper, and films obtained from vacuum-filtered pulps and model compounds were determined by the sessile drop method. Briefly, a 5 μl water droplet was placed on the paper or film surface. After 1 min, a photograph was taken using a smartphone (iPhone 11), and the WCA was measured using ImageJ software. Six droplets were analyzed for each sample. The means and the standard errors of WCAs were calculated and used for the plots.

Hydrophobic paper stabilities were evaluated by immersing modified A4/KPP paper in 100 mL of aqueous HCl (pH from 0 to 14), methanol, ethanol, isopropanol, toluene, or hexane for 5 h, removing it, and drying it in an oven at 60 °C for 2 h. The WCA was then determined. Moreover, Fe^{3+} modified A4 paper was conditioned at ambient conditions (i.e., ~25 °C, ~65 % humidity) for 6 months. The WCA of the conditioned sample was measured after specific periods.

The morphology and structure of the modified and nonmodified pulp fibers, paper, and model compounds were characterized by scanning electron microscopy (SEM, JEM-6110 LV, JOEL). The samples were sputter-coated with 30 nm platinum and operated at an accelerating voltage of 5 kV. Elemental distributions on samples were characterized using an energy dispersive X-ray spectroscopy (EDS) equipped on the SEM; the accelerating voltage was 15 kV, and the X-ray penetration depth was 3.7 μm.

The total metal contents (i.e., Zr and Fe) in modified KPPs were also determined by SEM-EDS under a 15 kV accelerating voltage. As a control, 0.01 M HCl-treated KPP was used. The paper was folded to the size of 1 cm^2 and a thickness of 100 μm. EDS scanning was conducted at a magnification of 100. The elemental content was determined in five distinct surface regions in each sample. The C, O, and Cl contents of KPP and modified KPP were determined too.

Metal ion leachability was determined by immersing 1 g of Fe^{3+} or Zr^{4+} modified KPP in 40 mL of acidic (pH 3), neutral (pH 7), and basic (pH 11) aqueous solutions for 1 h. Then, the concentration of leached Fe^{3+} or Zr^{4+} in the solution was measured using atomic absorption spectrometry and inductively coupled plasma mass spectrometry, respectively. The leaching tests were conducted over 4 cycles.

Before and after modification, the water absorbency of the paper was determined by the Cobb method with a self-designed setup with a ring outer diameter of 55 mm. The diameter of the tested paper was 50 mm. The measuring process was conducted according to the ASTM D3285-93 (2005).

Water retention of KPPs was determined as follows. Unmodified and metal ion-modified KPP samples (4 × 4 cm^2) were immersed in 100 mL distilled water for 1 to 164 h. After a set period, the sample was removed, and free water on the sample surface was removed using a dried tissue paper with a 500 g rod rolling on the sample surface. Then, sample weights were recorded, and the water retention was calculated according to the following equation:

$$Water\ retention(\%) = (M_t - M_0)/M_0 \times 100\%,$$

where M_0 represents the mass of the sample before absorbing the liquid, and M_t represents the mass of the sample after absorbing the liquid.

Fourier transform infrared spectroscopy (FTIR) analyses of paper and model compounds were recorded with a PerkinElmer Spectrum Two spectrometer using the attenuated total reflectance mode. An average of 20 scans with a 2 cm^{-1} resolution was used. The spectra were baseline-corrected using the Spectrum Quant software through the "data tune-up" function.

The surface elemental composition of the paper, before and after M^{x+}-modification, was investigated using a Thermo Scientific K-Alpha X-ray photoelectron spectroscopy (XPS) system with a monochromatic X-ray source at 1486.6 eV and a spot size of 400 μm. High-resolution spectra were obtained for Fe, Zr, O, C, and Cl, which were deconvoluted using the Thermo Scientific™ Advantage software.

Density functional theory (DFT) calculations were conducted using Q-Chem 5.3 and Spartan '20 software. The detailed calculation procedures are described in the Supporting Information.

3. Results and discussion

3.1. Hydrophobic paper by MIM

Paper is a thin mat of overlapping lignocellulosic fibers containing aligned cellulose microfibrils (Fig. 1**a**), which is hydrophilic because polar groups (e.g., OH and COOH) are present on the fiber surface [26]. In particular, "hairy" nanofibrils are fibrillated from the fibers during wood pulping and refining [7–9]. These "hairy" nanofibrils, with one end attached to the fiber's surface and a diameter range from 5 to 30 nm, are loaded with exposed surface polar groups (e.g., OH, C═O, etc.). These groups cause low water resistance in pulp and paper [9]. Paper rapidly absorbs water upon immersion in metal ion solutions while swelling the microfibrils. Simultaneously, metal ions are adsorbed on the nanofibrils by these polar groups, including OH, C═O, and COOH, through complexation [27–30]. During drying, the hanging nanofibrils self-assemble close towards the surface of the fiber as water evaporates. The complexed metal ions crosslink the nanofibrils by coordinating the nanofibril's surface oxygen-containing groups. This forms compact film-like structures (Fig. 1**a**). Metal ion coordination by the nanofibril oxygenated groups tightly binds oxygenated surface groups on the same and different nanofibrils holding them in close proximity in stable structures. This reduces the water affinity of lignocellulose nanofibrils and locks the nanofibrils into more compact and crosslinked structures that prevent water swelling. Fig. 1**b** includes photographs of the typical MIM process that converts conventional kraft packaging paper (KPP) into water-resistant hydrophobic paper. Unmodified KPP is hydrophilic and immediately absorbs water drops placed on it. In contrast, water drops remain almost spherical and stable on the surface of the Zr^{4+}, Al^{3+}, Fe^{3+}, or Fe^{2+}-modified KPPs, demonstrating that their surfaces are now hydrophobic. The measured WCAs (WCA, 1 min after dropping) of pristine and modified KPP are 0° and 110°–130°, respectively, suggesting MIM successfully causes the hydrophilic-to-hydrophobic transition of lignocellulosic papers. The MIM process also effectively modifies pulp which can then be directly molded into paper plates and cups (Fig. 1**c**). This demonstrates that the MIM process can be integrated with the paper-making process for manufacturing hydrophobic tableware.

3.2. Influence of metal ion modification conditions on the hydrophobicity of treated paper

Fig. 2**a** shows the WCAs of conventional KPP after 60 mM Fe^{3+} or Zr^{4+} solution immersions versus time, followed by oven drying at 60 °C for 2 h. After being immersed in the Zr^{4+} solution for only 1 s and then dried, KPP becomes hydrophobic with a WCA of 106 ± 3.3°. The contact angle rises to 124 ± 0.81° after 1 min of immersion and remains at ~130° as the immersion time is extended to 4 h. The Fe^{3+}-treated KPP (Fe^{3+}-KPP) also exhibits increased hydrophobicity, despite the lower WCAs of Fe^{3+}-KPP than those of Zr^{4+}-treated KPP (Zr^{4+}-KPP) early in the process (e.g., within the first-minute of immersion). After a 1 s Fe^{3+} immersion and then drying, the WCA of Fe^{3+}-KPP is 79.6 ± 9.9°. This increases to 109.9 ± 1.9° with the immersion time extended to 10 s. After 1 min immersion and then drying, the WCA of Fe^{3+}-KPP reaches 121.5 ± 0.2°, and then the WCA remains between 120 and 130° as the

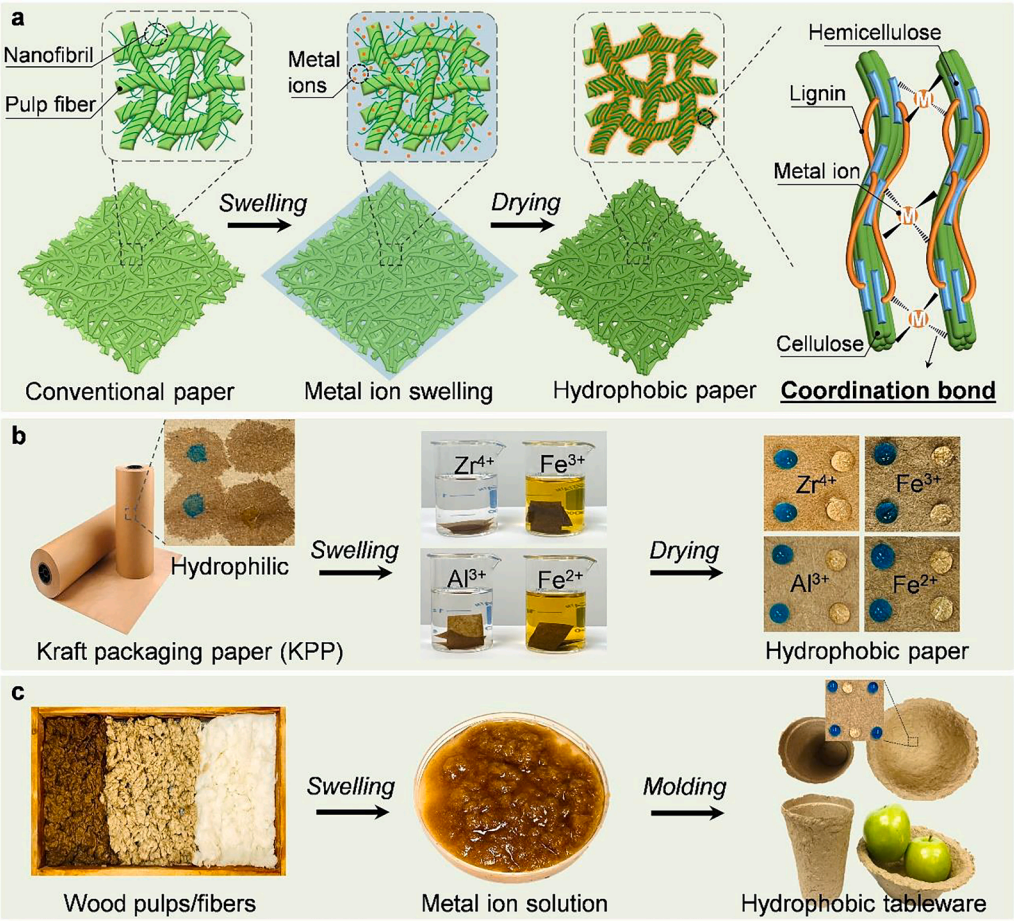

Fig. 1. A) Schematic illustration of the process and mechanism of hydrophobization of lignocellulose paper by MIM. Metal ions coordinate with lignocellulose's OHs and induced the self-assembly of pulp fibers' surface nanofibrils to form a compact surface with lower surface energy and hydrophobic characteristics. b, c) Photographs illustrate the MIM approach (i.e., swelling hydrophilic paper/pulp in 60 mM metal chloride solutions for 4 h, followed by drying/molding at 60 °C for 2 h) to prepare hydrophobic paper (b) and tableware (c). The blue drops are 20 ppm methylene blue solutions. (For interpretation of the references to colour in this figure legend, the reader is referred to the web version of this article.)

immersion time is extended to 4 h. Because 1 s M^{x+} immersion has already induced the wettability transition of KPP, simply spraying KPP with dilute Fe^{3+} or Zr^{4+} solutions also produced hydrophobic KPP (i.e., the WCA of Fe^{3+} and Zr^{4+} sprayed KPP after drying is 100° and 125°, respectively).

The time dependence of A4 copy paper's WCA upon 60 mM Zr^{4+} and Fe^{3+} immersions is shown in Figure S2**a**. Longer immersion times are required to achieve the wettability transition of A4 paper. For instance, 5- and 60-min immersions are needed for Zr^{4+} and Fe^{3+}, respectively, to convert pristine A4 paper to hydrophobic paper with a WCA of >120°. The difference in required immersion times between KPP and A4 paper can be attributed to their different chemical composition, i.e., KPP contains some hydrophobic lignin while A4 paper does not.

Fe^{3+} and Zr^{4+} solutions are acidic (pH 1–5 depending on the concentration) and contain anions (i.e., Cl^- for $FeCl_3$ and $ZrOCl_2$). This requires investigating the roles of acid solutions and anions on paper wettability change. Therefore, KPP, A4 paper, and kraft tissue paper (KTP) were treated with water and HCl solutions (10 mM, 50 mM, and 100 mM) using the same conditions for M^{X+} modification (4 h immersion followed by 60 °C for 2 h oven drying). In contrast with Fe^{3+}- and Zr^{4+}-treated KPP, KTP, and A4 paper, which all exhibited a WCA of >120°, both water- and HCl-treated papers remained hydrophilic with WCAs of 0° (Fig. 2**b**). Thus, the metal ions Fe^{3+} and Zr^{4+} are responsible for the paper's hydrophobicity.

The hydrophobic transition of lignocellulosic paper is metal ion concentration-dependent. Fig. 2**c** illustrates that immersion in 0.1 mM Fe^{3+} or Zr^{4+} does not endow KPP with hydrophobicity. Increasing Zr^{4+} concentration from 0.1 mM to 3 mM increased the WCA of KPP from 0° to 127.0 ± 2.2°, and it remained at 125 ~ 140° with Zr^{4+} concentrations from 10 mM to 200 mM. Further increasing the Zr^{4+} concentration caused the reduction of WCA to 109.0 ± 3.5°. A similar concentration-dependent trend is observed for Fe^{3+}-KPP. The KPP's wettability transition is attributed to the metal ion (e.g., Zr^{4+} and Fe^{3+}) complexation with hydrophilic groups (mostly –OH) of the cellulose, hemicellulose, and lignin components of the paper. When the concentration of metal ions is too low (e.g., 0.1 mM), there are not enough metal ion complexation sites to cause sufficient crosslinking and structural aggregation of nanofibrils, hence OH group availability to water to generate hydrophobicity. On the other hand, a concentrated metal ion solution may promote the excess deposition of the hygroscopic metal salts (e.g., Zr^{4+} or Fe^{3+} salts) onto the modified surfaces without enough further lignocellulose sites for complexation [31], thereby decreasing the WCA of the modified paper. A similar trend of metal ion concentration-dependent wettability was also observed (Figure S2**b**) for the A4 paper.

The hydrophobicity of metal-ion-modified papers is independent of the drying temperature. In a wide range of drying temperatures from 25 °C to 100 °C, the WCAs of Zr^{4+}- and Fe^{3+}-KPP (Fig. 2**d**) were all above 120° with no significant differences. Similar temperature-independent wettability changes were also observed for Zr^{4+}- and Fe^{3+}-modified A4 paper (Figure S2**c**). MIM is an effective "universal" method for rendering various hydrophilic papers to become hydrophobic, including A4 paper, writing paper (WP), KPP, cardboard, KTP, and newspaper (Fig. 2**e**) with WCAs between 120 and 145°.

The lignocellulosic paper's wettability transition is metal ion-dependent, as shown in Fig. 2**f**. Using A4 paper, Zr^{4+} and Fe^{3+} modifications exhibited the highest WCA of ~ 130°, followed by Y^{3+} (123.3 ± 2.4°), Al^{3+} (121.1 ± 2.4°), and Fe^{2+} (119.0 ± 1.4°). Cu^{2+} and Co^{2+} treated A4 paper also improved hydrophobicity, but their WCAs were below 90°. However, Li^+, Na^+, and Ca^{2+} treated papers remained

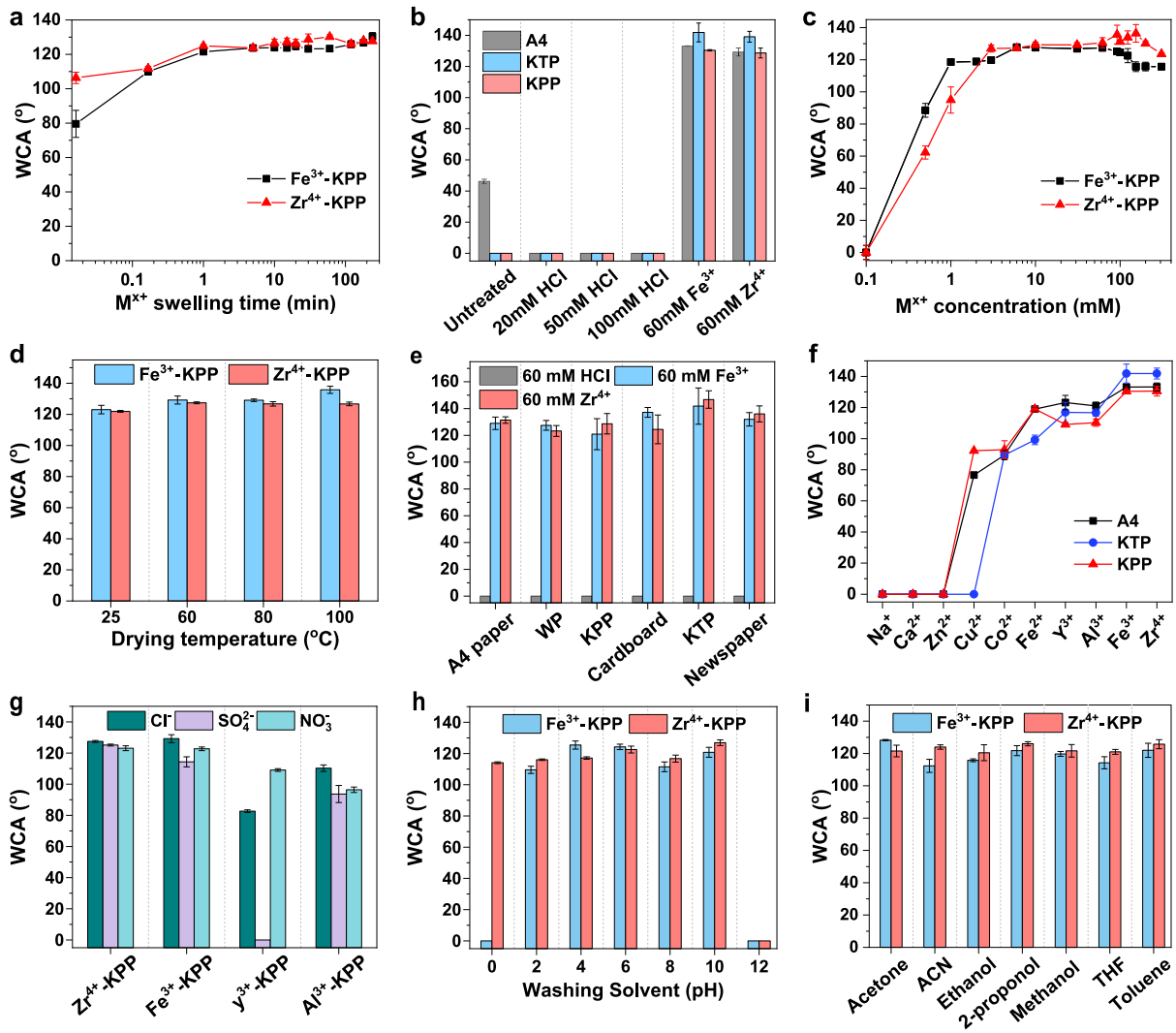

Fig. 2. A) WCAs of Fe^{3+}- and Zr^{4+}-KPP versus time. b) WCAs of KPP, A4 paper, and KTP after being treated with different solutions, including HCl, Fe^{3+}, and Zr^{4+}. c) WCAs of Fe^{3+}- and Zr^{4+}-KPP versus metal ion concentrations. d) WCAs of Fe^{3+}- and Zr^{4+}- KPP versus drying temperatures. e) WCAs of HCl, Fe^{3+}, Zr^{4+} treated conventional papers. f) WCAs of KPP, KTP, and A4 paper after modifying with different metal ion solutions, in which the counter anion was NO_3^- for Co^{2+} and Y^{3+}. g) WCAs of Zr^{4+}, Fe^{3+}, Y^{3+}, and Al^{3+} treated KPP with different counter anions. h) WCAs of Zr^{4+} or Fe^{3+} modified KPP after 5 h washing with different pH aqueous solutions. i) WCAs of Zr^{4+} or Fe^{3+} modified KPP after 5 h washing with different organic solvents. Unless specified, the concentration of the metal ion solution was 60 mM, the swelling time was 4 h, the metal ion solution's counter anion was Cl^-, and the drying condition was 60 °C for 2 h. WCAs of papers were measured after the papers were dried.

hydrophilic with WCAs of 0°. Similar trends are observed for KPP and KTP. The complexation between M^{x+} and lignocellulose's OHs is the key to the papers' wettability transition. It is known that the metal cation's binding energy (or ionization potential) plays an important role in the coordination between M^{x+} and electron donors such as hydroxyl-, carboxylic-, and amine-containing organic compounds [32,33]. We speculate that the M^{x+} with higher ionization potential might lead to higher WCAs of M^{x+}-modified papers. To demonstrate this, we plotted the figures of WCAs versus metal cation's ionization potential values [33]. As shown in Figure S3, the WCAs of modified papers positively correlate with the ionization potentials of metal cations used for paper modification. For instance, the WCAs versus ionization potential plots fit well to a linear regression model with a coefficient of determination (R^2) of 0.832 ~ 0.928 for all tested papers (e.g., A4, KTP, and KPP). This result confirms that metal cation's ionization potential is important for lignocellulose materials' wettability transition.

Fig. 2g depicts the influence of counter anion (Cl^-, NO_3^-, SO_4^{2-}) in metal cation solutions on WCAs of modified KPP. For the same metal cation, WCAs of modified KPP vary with the counter anions present in the solution. For instance, $FeCl_3$-treated KPP gave the highest WCA (130.6 ± 2.2°), followed by $Fe(NO_3)_3$-treated KPP (126.1 ± 2.4°) and $Fe_2(SO_4)_3$-treated KPP (112.4 ± 2.8°). One-way analysis of variance (ANOVA) results indicates that the differences among this Fe^{3+}-treated KPP are significant (i.e., $P \leq 0.05$). The same trend is observed for Al^{3+}-treated KPP ($P \leq 0.05$). For Zr^{4+}, $ZrOCl_2$-treated KPP gave the highest WCA (130.3 ± 1.5°), followed by $Zr(SO_4)_2$ (128.0 ± 2.0°) and $Zr(NO_3)_4$ (125.3 ± 1.9°), although the differences are not significant (i.e., $P = 0.18$). For Y^{3+}, $Y(NO_3)_3$ treated KPP shows highest WCA of 112.4 ± 2.2°, followed by YCl_3 (89.8 ± 4.8°). This could be attributed to the poor solubility of YCl_3, which is barely soluble in water. As shown in Figure S4, the $Y(NO_3)_3$ solution is transparent, suggesting it is fully dissolved, while the YCl_3 solution is cloudy, indicating it is not fully dissolved. Despite $Y_2(SO_4)_3$ being soluble in water and giving a transparent solution (Figure S4), $Y_2(SO_4)_3$ treatment did not produce KPP with hydrophobic characteristics (WCA = 0°). The reason for this is unclear. Overall, $FeCl_3$, $ZrOCl_2$, and $AlCl_3$ are the best salts for lignocellulose materials' wettability transition.

The hydrophobicity of metal-ion-modified papers persisted after 4 h

of aqueous immersion over a wide pH range from 2 to 10 (Fig. 2**h**). Even after 4 h of 1 M HCl solution immersion and drying, Zr^{4+}-KPP still exhibits a high WCA of 114.1 ± 0.6°. Although Fe^{3+}-KPP loses the hydrophobicity after immersion in 1 M HCl for 4 h, its hydrophobicity was preserved after 4 h immersion in pH 2–10 solutions. This implies that the coordination between Zr^{4+}/Fe^{3+} and lignocellulosic fibers is stable over a wide range of solution pHs from strongly acidic to moderately basic. However, after immersion with strong alkaline solutions, Zr^{4+} and Fe^{3+}-KPP lose their hydrophobicity (pH ≥ 12). This is attributed to the swelling of lignocellulosic fibers in the strong alkaline environment, which might alter the molecular structure of cellulose, hemicellulose, and lignin, thereby affecting the coordination [34]. Similar results were observed for Fe^{3+}-A4 (Figure S5**a**), where its hydrophobicity was retained after 4 h immersion in pH 0–10 solutions but lost after immersion in pH ≥ 12 solutions. The hydrophobic papers are resistant to organic solvent soaking. As shown in Fig. 2**i**, Zr^{4+}- and Fe^{3+}-KPP remain hydrophobic (WCA of 120 ~ 130°) after a 4 h immersion at ambient temperatures in various solvents, including methanol, ethanol, isopropanol, toluene, hexane, acetonitrile (ACN), and tetrahydrofuran (THF). Similar results were observed for Fe^{3+}-A4 (Figure S5**b**). Furthermore, hydrophobic paper is durable. As shown in Figure S5**c**, after being stored at ambient conditions for 6 months, Fe^{3+}-A4 remains hydrophobic with a WCA of 133°.

3.3. Water resistance and wet strength of hydrophobic papers

MIM-derived hydrophobic papers display good water resistance compared with conventional paper. As shown in **Figure S6**, the unmodified KPP-based origami boat gets wet within 30 s upon water exposure and sinks after 60 s (**Video S1**). In contrast, the corresponding origami boat fabricated from Fe^{3+}-KPP remains water impermeable and floating after 30 d of water exposure. To quantify the water resistance of hydrophobic papers, the Cobb values (Fig. 3**a**) and water retention values (**Figure S7**) of KPP, Fe^{3+}-KPP, and Zr^{4+}-KPP were measured and compared. The Cobb test evaluates the paper's resistance to water penetration by a one-face water exposure experiment, which measures the amount of water absorbed within a few minutes. After 60 s of exposure, the $Cobb_{60}$ value of KPP has already reached 63.1 g/m^2. Increasing the exposure time to 300 s results in a slightly higher $Cobb_{300}$ of 69.4 g/m^2. In contrast, the $Cobb_{60}$ values of Fe^{3+}-KPP (9.9 g/m^2) and Zr^{4+}-KPP (8.7 g/m^2) are five times smaller than that of KPP. Increasing exposure time to 300 s slightly increased these quantities to Fe^{3+}-KPP

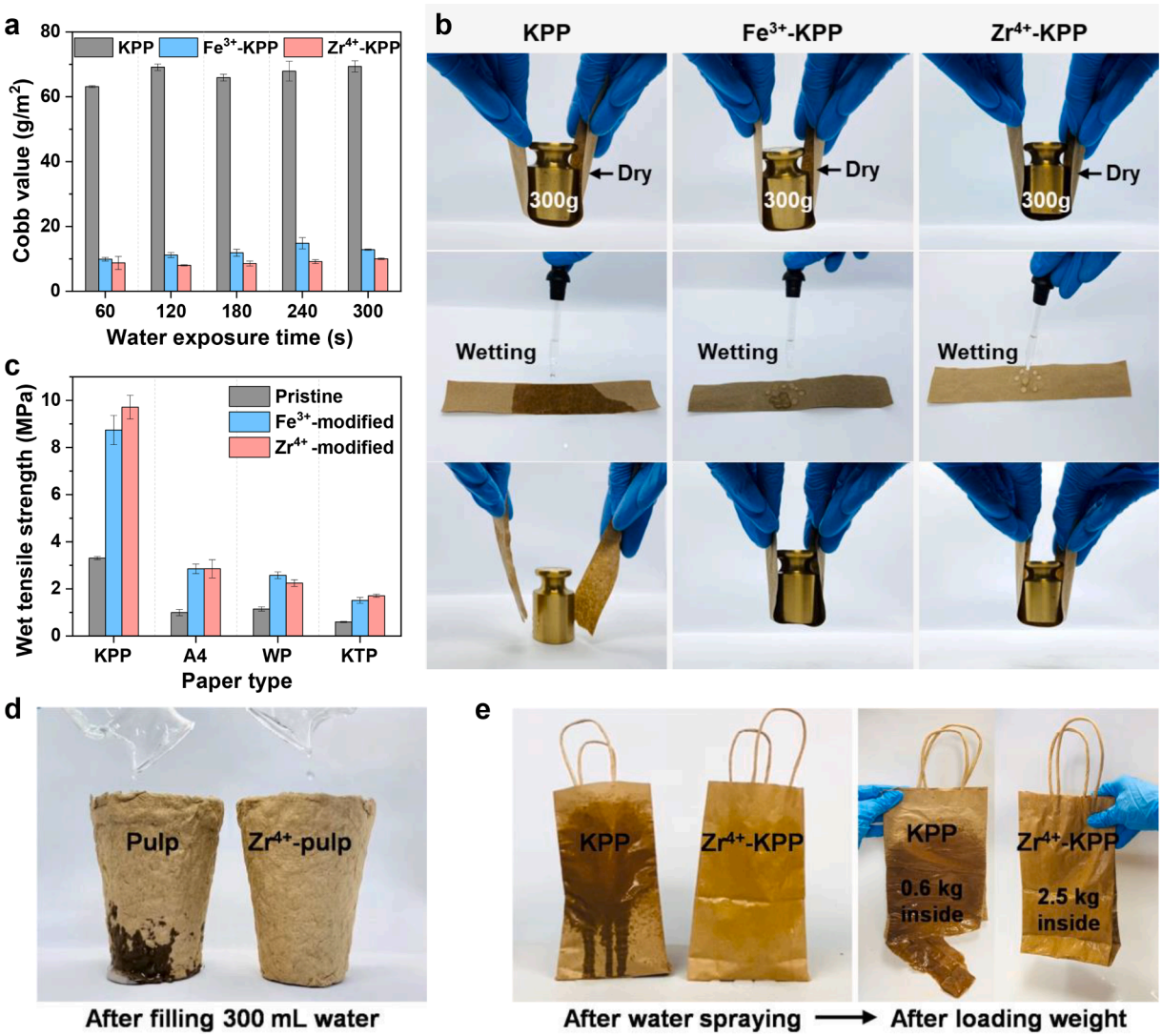

Fig. 3. Water resistance, water absorptiveness, and strength of hydrophobic paper and tableware. a) Comparisons of Cobb values of KPP, Fe^{3+}-KPP, and Zr^{4+}-KPP measured at 60–300 s. b) Photographs show the mechanical performance of KPP, Fe^{3+}-KPP, and Zr^{4+}-KPP in dry and wet states. c) Wet tensile strength of conventional papers before and after metal Fe^{3+} and Zr^{4+}modification. d) Photographs show water impermeability of Zr^{4+}-pulp paper cups after filling 300 mL of water. e) Photographs show Zr^{4+}-KPP packaging bag remains strong after water spraying.

(12.8 g/m^2) and Zr^{4+}-KPP (10.0 g/m^2), but these values are still five times lower than that of KPP. The water retention rate measures the amount of water trapped in the paper's pores after water absorption, which can be used to quantify a paper's long terms water resistance. Conventional KPP shows a water retention rate of 85 % after 1 h water immersion, which increased to 145 % after a 7d water immersion. However, Fe^{3+}-KPP and Zr^{4+}-KPP show lower water retention rates of 33 % and 65 % after 1 h and 7 d water immersion, respectively. This further confirmed the long-term water resistance of hydrophobic papers.

Hydrophobic paper exhibits superior wet strength resulting from its excellent water resistance. When a few drops of water wetted the KPP strip (2 cm × 10 cm), it could not bear as heavy a load (i.e., 300 g) as it does when dry (i.e., 300 g) (Fig. 3**b**). In contrast, Fe^{3+}-KPP and Zr^{4+}-KPP could bear a heavy load, whether dry or wet. As shown in **Figure S8**, Fe^{3+}- and Zr^{4+}-treated papers (e.g., A4, KPP, KTP) exhibit dry tensile strengths comparable to their untreated counterparts without statistically significant differences. In comparison, the wet tensile strength of Fe^{3+}- and Zr^{4+}-papers was significantly (2–3 times) higher than those of unmodified papers (Fig. 3**c**). To demonstrate the potential application of metal-ion-modified papers and pulps, we fabricated paper cups and paper bags using Zr^{4+}-pulp and Zr^{4+}-KPP, respectively. Fig. 3**d** shows a molded Zr^{4+}-pulp cup with good water impermeability that does not leak after storing 150 mL water for 1 h. In contrast, water quickly leaked from the unmodified pulp-molded cup within 2 min (**Video S2**). Similarly, after spraying with water, the Zr^{4+}-KPP bag remains mechanically robust and can hold a weight of 2.5 kg without breaking. However, the conventional KPP bag broke when holding a 0.6 kg weight (Fig. 3**e**). Additionally, the Zr^{4+}-pulp tableware can store hot water, milk, orange juice, and coffee. As can be seen from Video 1, no leaking was observed after pouring 70–80 °C hot water into the Zr^{4+}-pulp cup for 15 min. Similarly, no leaking was observed when storing hot milk, orange juice, and hot coffee in Zr^{4+}-pulp tableware (**Figure S9**).

3.4. Economic feasibility, safety, biodegradability, and recyclability

The metal content of hydrophobic Fe^{3+}- and Zr^{4+}-KPPs was determined to evaluate the economic feasibility of the MIM process for hydrophobic paper production. The metal contents within hydrophobic papers (Fig. 4**a**) are low, i.e., < 0.6 wt% for Fe^{3+}-KPP and <1.3 wt% for Zr^{4+}-KPP, respectively. These values agree with the measured mass gain (**Figure S10**) of 1–2 wt% after treating KPP with 60 mM Fe^{3+} or Zr^{4+} for 4 h. Moreover, the metal content of hydrophobic paper increased as the concentration of the metal ion solution rose logarithmically during the treatment. For instance, a Fe^{3+} solution concentration tenfold increments from 10 mM to 100 mM only caused the iron content in Fe^{3+}-KPP to rise from 0.28 wt% to 0.55 wt%. Furthermore, the WCAs of Fe^{3+}- and Zr^{4+}-KPPs remained >120° even when the Fe^{3+} or Zr^{4+} contents in the paper were as low as 0.3 wt%. These values are comparable with conventional 0.5 wt% AKD- and ASA-sized hydrophobic paper [2]. The cost of metal salts is lower than the organic sizing agents (i.e., $FeCl_3$: US $500/metric ton, AKD: US$2,400/metric ton, price from Alibaba). When 0.5 wt% of Fe^{3+} and AKD are used as internal sizing agents for paper hydrophobization, the costs of Fe^{3+} (i.e., US$2.5 per metric ton pulp) is five times lower than that of AKD (i.e., US$12 per metric ton pulp). Thus, the MIM process is a promising and economically feasible method to produce water-resistant packaging paper and tableware.

The stability of metal ion complexes within the modified hydrophobic papers was studied using a cyclic leaching test to evaluate the

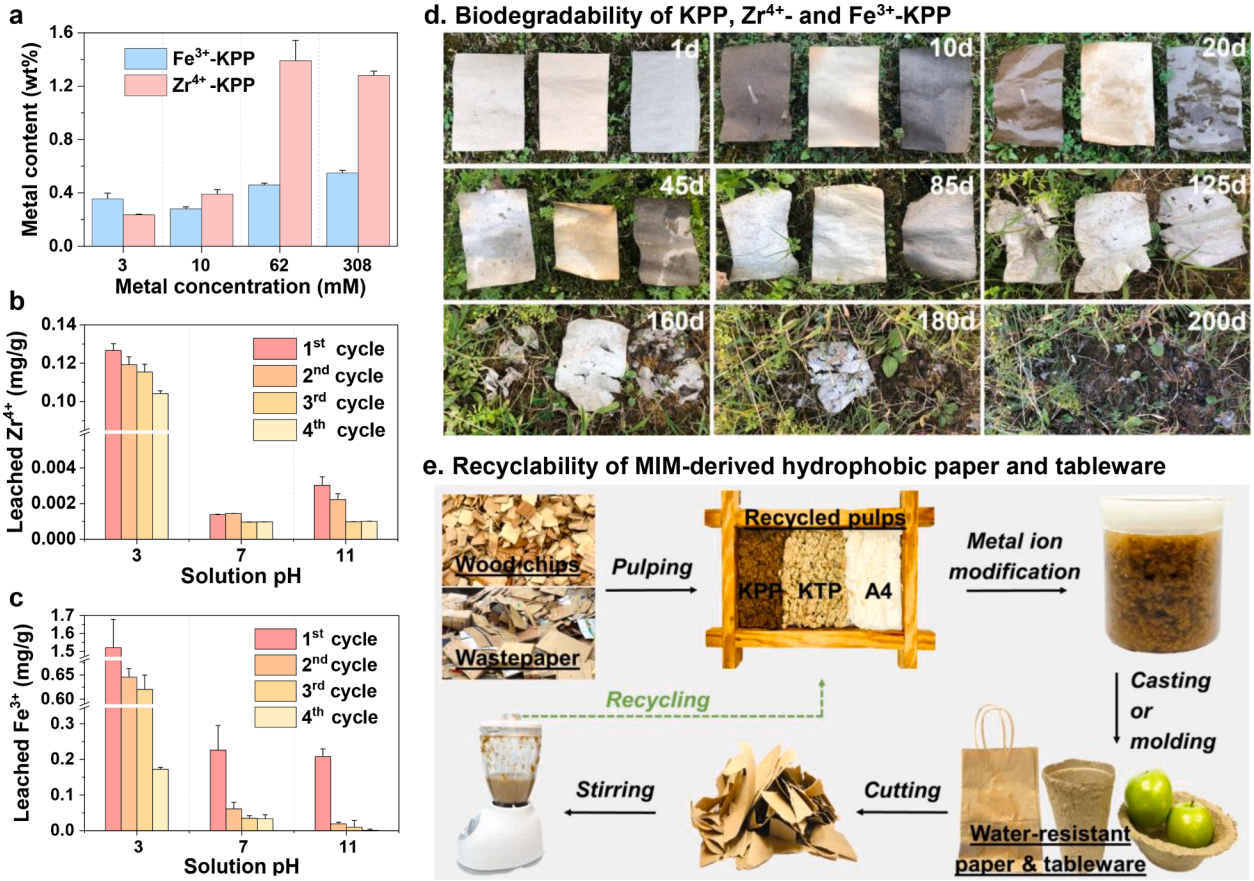

Fig. 4. Metal ion content, stability, biodegradability, and recyclability of hydrophobic paper and tableware. a) Effect of solution metal ion concentrations on the Fe and Zr loadings of modified hydrophobic KPPs. b, c) The Zr^{4+} (b) or Fe^{3+} (c) leaching of M^{x+}-KPP after 1 h immersion in an aqueous solution at pH 3,7, and 11. d) The biodegradability tests of the KPP (left, paper size is 8 × 11 cm), Zr^{4+}- (middle), and Fe^{3+}-KPP (right) under an outdoor no-soil contact environment.

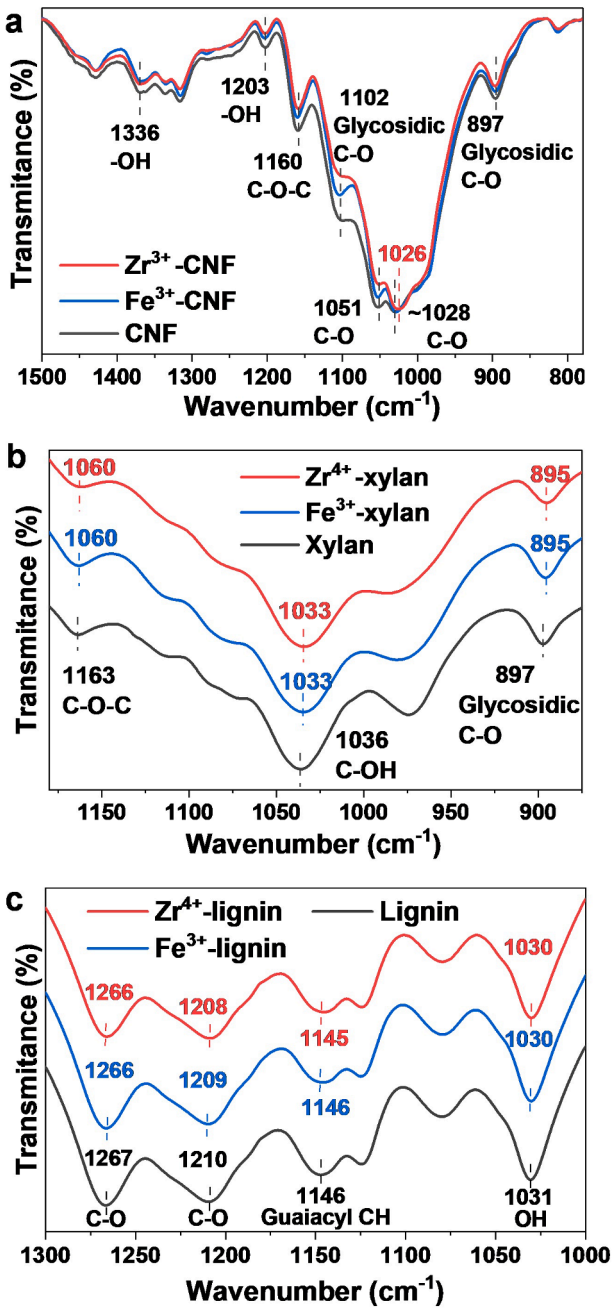

Fig. 5. a-c) FTIR spectra of CNF (a), xylan (b), and lignin (c) before and after Fe^{3+} and Zr^{4+} modification.

safety of the modified paper. Specifically, 1 g of Zr^{4+} or Fe^{3+}-KPP was shredded and immersed in water at pH 3, 7, and 11 for 1 h. The leached metal ion concentrations are shown in Fig. 4**b**. In the first cycle, <0.003 mg of Zr^{4+} was leached from 1 g of Zr^{4+}-KPP into neutral and basic leaching solutions. In the third cycle, the amount of leached Zr^{4+} dropped to <0.001 mg/g. Zr^{4+} leaching rose in the pH 3 solution but was still lower than 0.15 mg/g. The daily human uptake of Zr from food and beverage is as high as 125 mg [35]. So, the Zr^{4+} leached from Zr^{4+}-KPP is negligible. Fe^{3+} leaching from Fe^{3+}-KPP was higher (Fig. 4**c**) than from Zr^{4+}-KPP. For instance, during the first cycle leaching test, the amounts of Fe^{3+} leached into pH 3, 7, and 11 water solutions were 1.52, 0.22, and 0.21 mg/g, respectively. Similar to Zr^{4+}, the Fe^{3+} leaching decreased in later testing cycles. In the fourth leaching cycle, the quantities of Fe^{3+} leached into pH 3,7, and 11 solutions were 0.17, 0.03, and 0.001 mg/g, respectively. Since Fe is a necessary trace element for humans and the median dietary intake of iron is 12–18 mg/day [36,37], exposure to Fe^{3+} leached from modified paper is acceptable. Therefore, Fe^{3+} and Zr^{4+} modified hydrophobic lignocellulosic materials are safe for non-food and food contact packaging applications.

Hydrophobic paper, like conventional paper, is also biodegradable. For comparison, KPP, Zr^{4+}- and Fe^{3+}-KPPs were placed on grass and exposed to the sun, wind, and rain (Starkville, MS, U.S., from February 2022 to September 2022). Their morphologies over time were monitored (Fig. 4**d**). Unmodified hydrophilic KPP is readily wetted by dew (Fig. 4**d, 10** d). However, Fe^{3+}- and Zr^{4+}-KPP remained hydrophobic after 10 d of natural weathering. Dew drops remained spherical on the Fe^{3+}- and Zr^{4+}-KPP surfaces, see **Figure S11** (a magnified image of Fig. 4**d, 10** d). After 20 d of natural weathering, the Fe^{3+}- and Zr^{4+}-KPP remained impermeable, but surface dew drops no longer retained a spherical shape. After 45 d of natural weathering, black spots are observed on the surface of unmodified KPP, probably due to sunlight or microorganism degradation. Meanwhile, Fe^{3+}- and Zr^{4+}-KPP slowly lose their water impermeability and become wettable. Biodegradation-induced black spots on Fe^{3+}- and Zr^{4+}-KPP were observed after 85 d. Unmodified KPP is completely biodegraded after 165 d. In comparison, Fe^{3+}- and Zr^{4+}-KPP are more durable but were also completely degraded after 180 and 200 d, respectively. This is a good balance between durability and biodegradability. Hydrophobic paper is both stable and durable under working conditions yet easily degraded under natural soil or outdoor conditions, which is appealing for designing next-generation sustainable, biodegradable, and high-performance packaging materials. Additionally, Fe^{3+}- and Zr^{4+}-KPP placed in contact with outdoor soil biodegraded within 130 d (**Figure S12**).

M^{X+}-modified hydrophobic lignocellulosic products are recyclable. The end-of-life hydrophobic paper and tableware can be broken back down into the metal ion-containing pulp slurry by mechanical stirring, allowing it to be recycled (Fig. 4**e**). Retained stable metal-lignocellulose coordination bonds render this recycled pulp to be hydrophobic. **Figure S13** shows that lignocellulosic paper produced from first-round recycled pulp has a WCA of 135°. However, after the second recycling round, the recycled pulp lost its hydrophobicity (WCA = 40°). This might result from the intense mechanical blending that has caused new fibrillation to occur on the fibers of recycled pulps [7]. Such fibrillation would generate more nanofibrils on the pulp surface, increasing the pulp's hydrophilicity. Furthermore, upon again treating the second-round recycled pulp with metal ion solution (e.g., 60 mM Fe^{3+} or Zr^{4+}), its hydrophobicity was reestablished (WCA = 135°), as shown in **Figure S14**.

3.5. Metal lignocellulose interactions and MIM mechanism

FTIR spectra of conventional paper before and after modification are recorded and compared (**Figure. S15a**). Characteristic peaks of cellulose (e.g., 1372, 1201, 1160, 1105, 1059, 1033, and 896 cm^{-1}, etc.) [38,39] and hemicellulose (i.e., ~1734 and ~1268 cm^{-1}) [38] are observed in the FTIR spectra of all the paper samples, while lignin fingerprint peaks (e.g., 1593, 1511, 1450, 1266, and 814 cm^{-1}) [39,40] are observed only for KPP, KTP, and cardboard. This is because the chemical composition of different paper types varies with their manufacturing procedures. A4 and WP are usually fabricated from bleached kraft pulps where lignin has been removed [41], while KTP, KPP, and cardboard are typically produced from unbleached kraft pulps where lignin is partially retained [41–43]. After Fe^{3+} and Zr^{4+} modification, several changes are observed in the FTIR spectra of paper samples. For instance, hemicellulose-related (~1734 cm^{-1}, corresponding to C═O stretching in O═C-OH group) [38] and lignin-related (1266 cm^{-1}, corresponding to aromatic carbon to methoxy oxygen **sp^2 C—O—CH_3** stretching in guaiacyl ring) [44] bands are shifted to lower wavenumbers (**Figure S15b and c**). To elaborate on metal-lignocellulose interactions, we modified lignocellulose model compounds, i.e., cellulose nanofiber (CNF), xylan (the main component of hemicellulose), and kraft lignin with Fe^{3+} and Zr^{4+} . The

changes in their FTIR spectra were monitored (**Figure S16**). Fig. 5**a** shows the regions of FTIR spectra with the most significant changes for each compound. For CNF, the band at 1028 cm^{-1} corresponding to sp^3 C—O vibrations of cellulose, is found shifted to ~1026 cm^{-1} after Fe^{3+} and Zr^{4+} modification. Coordination of the oxygen lone pairs to Fe^{3+} or Zr^{4+} causes a reduction in the C—O peak wavenumbers. Moreover, intensity reductions are observed for cellulose's C—O stretching of C-OH groups (~1336 and 1203 cm^{-1}), C—O—C (1160 cm^{-1}), glucose unit (1102 and 897 cm^{-1}), and C—O (1051 cm^{-1}) vibration bands. These combined results indicate that Fe^{3+} and Zr^{4+} ions have chelated with cellulose's OH groups and ring oxygens [45]. For xylan, glycosidic C—O stretching (897 cm^{-1}), C—O stretching of C-OH groups (1036 cm^{-1}), and C—O—C stretching (1601 cm^{-1}) are found to shift to lower wavenumbers. This confirmed the coordination of metal ions with xylan's OH groups and ring oxygens. Moreover, the C═O stretching peak at 1741 cm^{-1} (C═O stretching in the O═C-OH group) was subject to an intensity enhancement (**Figure S16b**), implying Fe^{3+} and Zr^{4+} coordinate to the C═O oxygen atom. Stretching vibrations of lignin's aromatic carbon to methoxy oxygen (**sp^2 C—O—CH_3**) stretching in guaiacyl ring (1210 and 1267 cm^{-1}), phenolic hydroxyl C—O (1363 cm^{-1}, in **Figure S16c**), aliphatic hydroxyl C—O (1031 cm^{-1}), and guaiacyl C—H (1147 cm^{-1}, in-plane deformation) [46,47] are subjected to lower wavenumber peak shifts. These shifts indicate oxygen lone pair coordination to metal ions by lignin's ring oxygens and OH groups.

XPS was used to further investigate the interactions between metal ions and lignocellulosic papers. Wide-scan XPS spectra of KPP (Fig. 6**a**) and KTP (**Figure S18a**) show C, and O peaks, while Fe and Zr peaks are observed in the Fe^{3+} and Zr^{4+} modified paper spectra, respectively. In lignocellulosic materials, there are two types of O atom oxidation states, the C—O of hydroxyls and ethers and the C═O of carbonyl and carboxylic groups. Fig. 6**d** displays the O 1 s peak of pristine KPP, deconvoluted to two peaks at binding energies of 531.90 and 532.65 eV that are assigned to the C—O and C═O groups, respectively. However, the O 1 s peak of Fe^{3+}-KPP can be deconvoluted to three peaks at 531.30, 532.30, and 532.95 eV that correspond to Fe—O—C [48,49], C—O, and C═O groups, respectively. The new Fe—O—C deconvolution peak and the shifting of the C—O (i.e., from 531.90 to 532.30 eV) and C═O (i.e., from 532.65 to 532.95 eV) peaks to higher binding energies indicate that Fe^{3+} coordinates to both C—O and C═O group oxygen atoms. Similarly, the O 1 s peak of Zr^{4+}-KPP was also deconvoluted into three peaks belonging to Zr—O—C (531.80 eV) [50], C—O (532.30), and C═O (532.95 eV), respectively. This also supports the coordination between

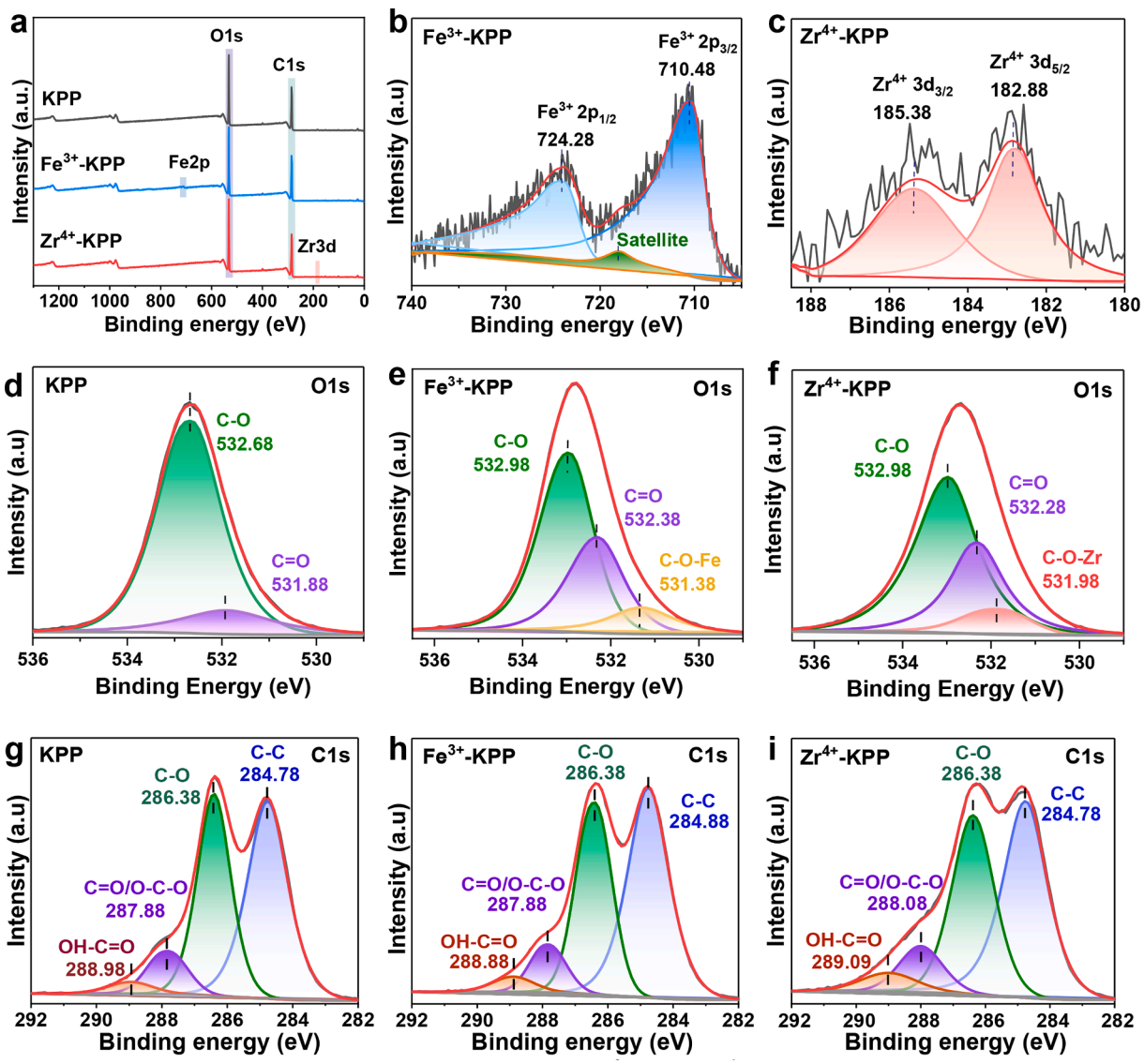

Fig. 6. XPS spectra of KPP before and after Fe^{3+}- or Zr^{4+} modification. a) Wide-scan XPS spectra of KPP, b) Fe 2p of Fe^{3+}-KPP, c) Zr 3d of Zr^{4+}-KPP. d-i) High-resolution XPS spectra of KPP and modified KPPs: d) O1s of KPP, e) O1s of Fe^{3+}-KPP, f) O1s of Zr^{4+}-KPP, g) C 1 s of KPP, g) Fe^{3+}-KPP, h) and Zr^{4+}-KPP, i).

Fe^{3+} ions and the oxygens in C—O and C═O groups.

C 1 s spectra of KPP and modified KPP were deconvoluted to C—C, C—O, C═O, and O-C═O peaks, as shown in Fig. 6**g, h, and i**. The overall C 1 s spectra exhibited slight shifts to higher binding energies, but no noticeable peak shifting was observed for the deconvoluted peaks. The peaks of the corresponding metal elements were also observed in the Fe 2p and Zr 3d spectra of the Fe^{3+}- and Zr^{4+}-KPP samples (Fig. 6**b and c**), respectively. Moreover, both Fe^{3+} $2p_{3/2}$ (710.30 eV) and Zr^{4+} $3d_{3/2}$ (182.78 eV) peaks of modified KPP shifted to lower binding energies compared to that of $FeCl_3$ (711.80 eV) [51] and $ZrOCl_2$ (183.00 eV) [52]. This is consistent with oxygen coordination to both Fe^{3+} and Zr^{4+}, which raises electron density on the metal ions, lowering binding energies.

The surface morphology and microstructure of KTP before and after metal ion modification are characterized. Fig. 7**a** shows that KTP has an isotropic net-like structure that consists of randomly oriented lignocellulosic fibers. The fiber surfaces contain many loosely arranged nanofibrils that are generated during pulp fibrillation (Fig. 7**b**) [53], generating fibers with high porosity that are highly hydrophilic, promoting water absorption [9]. After modification, the Fe^{3+}-KTP exhibits a smoother surface (Fig. 7**c**). The "hairy" nanofibrils self-assemble into a compact film covering the parent fiber's surface (Fig. 7**d**), where the coordinated Fe^{3+} ions are evenly distributed on the fiber surface and crosslink the lignocellulose nanofibrils (Fig. 7**i**). Dilute HCl immersion and drying also induced the self-organization of nanofibrils, resulting in a smoother and more compact KTP surface (**Figure S19**), but HCl treatment does not make KTP hydrophobic (Fig. 2**b**).

Similarly, nanofibril self-assembly also occurred on Fe^{3+}-KPP (Fig. 7**f**) and Fe^{3+}-A4 (Fig. 7**h**). Both exhibited smoother and more compact surface morphologies than untreated KPP (Fig. 7**e**) and A4 (Fig. 7**g**). No metal salt (i.e., $FeCl_3$) (nano) particle deposition was observed on the paper's surface after treatment. Moreover, micron-sized sizing agents (i.e., calcium carbonate, yellow circle marked regions in Fig. 7**g**), which were used for improving the water resistance of A4, were removed after Fe^{3+} treatment (Fig. 7**h**). Furthermore, elemental mapping spectra for C, O, Fe and Cl (in Fig. 7) also show the uniform distribution of Fe^{3+} in Fe^{3+}-KPP and Fe^{3+}-A4 paper. The Fe to Cl atomic ratios of Fe^{3+}-treated papers are around 1:1.2, which is lower than that of $FeCl_3$ salt (i.e., 1:3), further confirming that the paper's hydrophobization was not because of metal salt deposition.

The combined evidence indicates that the metal ion-induced self-assembly of nanofibrils is responsible for the wettability reduction of lignocellulosic materials. Metal ions consumed lignocellulosic fibers' polar groups (i.e., –OH, C═O, and COOH) through coordination, which decreased the fibers' surface energy and water affinity. Furthermore, the strong metal ion coordination interactions and crosslinks reduce nanofibril flexibility and dispersibility in water, promoting self-assembly to form denser and less porous structures [23]. This lead to good water resistance and hydrophobicity.

3.6. DFT stimulations

The interactions between metal ions and lignocellulose model compounds (i.e., cellulose, hemicellulose, and lignin) were also studied by a minimal molecular model using DFT with an implicit solvation model. The optimized structures for interactions between Fe^{3+} and the individual monomeric units of cellulose, hemicellulose, and lignin are shown in Fig. 8**a**. DFT calculations confirm that the Fe^{3+} coordination

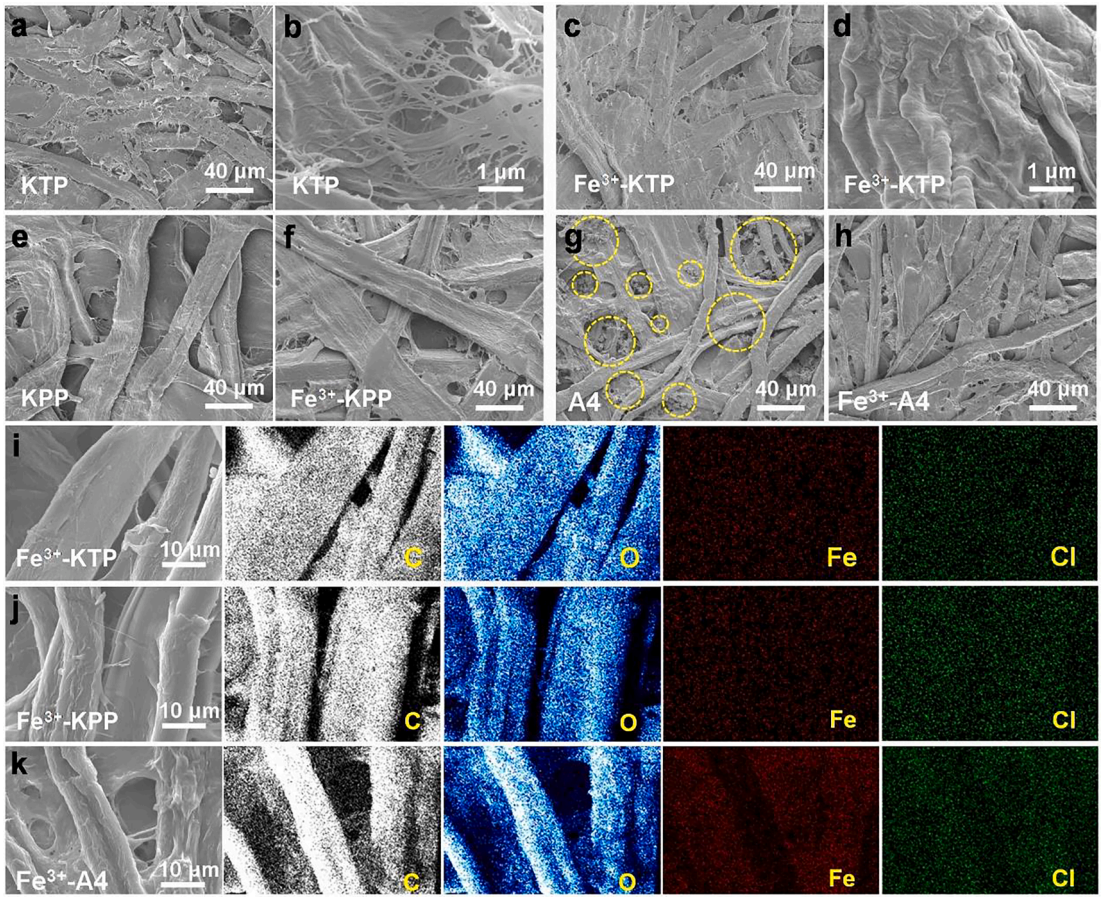

Fig. 7. (a-h) SEM characterization shows Fe^{3+}-treated KTP, KPP, and A4 have a smoother and more compact microstructure than the pristine paper; (i-k) SEM elemental mapping spectra show the uniform distribution of Fe^{3+}-treated KTP, KPP, and A4. The paper modification was carried out by immersing KTP, KPP, or A4 paper in an aqueous (60 mM) $FeCl_3$ solution for 4 h, followed by drying at 60 °C for 2 h.

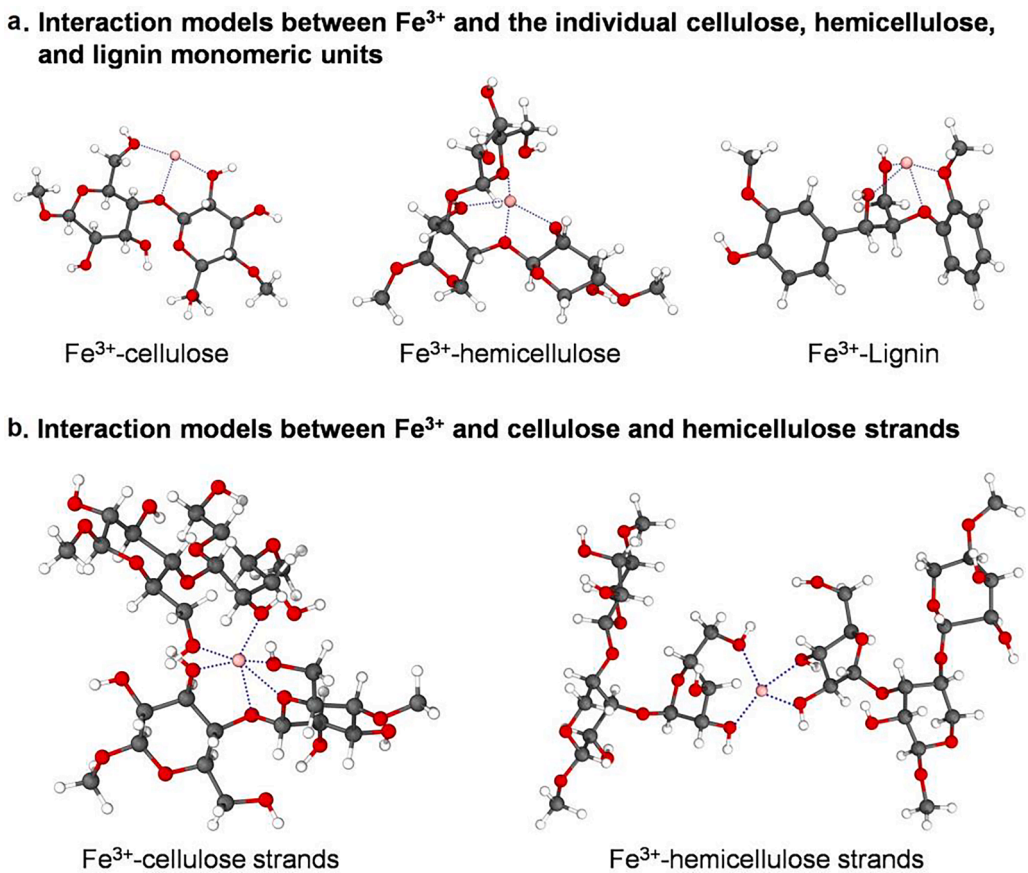

Fig. 8. A) Optimized structures of cellulose, hemicellulose, and monomeric lignin units interacting with Fe^{3+}. b) Optimized structures of Fe^{3+} coordinate with a pair of cellulose and hemicellulose strands.

sites on cellulose and hemicellulose are glycosidic and hydroxyl oxygens. In comparison, the coordination sites on lignin are the oxygen atoms of β-O-4 bonds and methoxy and hydroxyl groups. This agrees with the FTIR and XPS observations. These DFT calculations gave binding energies (E_{MB}) between Fe^{3+} and cellulose, hemicellulose, and lignin structures of –2869.6, –3175.0, and –2982.2 kJ/mol, respectively. Fe^{3+} has the highest coordination affinity for hemicellulose, followed by lignin and cellulose. This result suggests why more time is required to convert A4 paper to hydrophobic paper than KPP (Fig. 2**a** and Figure S2**a**) since KPP contains more hemicellulose and lignin.

To elaborate the self-assembly mechanism of lignocellulose nanofibrils upon metal coordination, the interactions between Fe^{3+} and a pair of cellulose or hemicellulose strands (monomeric units) were further investigated by DFT. As shown in Fig. 8**b**, Fe^{3+} forms a six-coordinate complex with two cellulose strands (monolayer). The calculated binding energy for a Fe^{3+}-chelated cellulose monolayer is –733.4 kJ/mol, which is more negative than the original binding energy of a cellulose monolayer without Fe^{3+} through just hydrogen bonding (–91.0 kJ/mol). Owing to its more negative binding energy, the Fe^{3+}-chelated cellulose monolayer is more stable than the pristine H-bonded cellulose strands and is less susceptible to disruption by water. In other words, water swells pristine cellulose monolayers but not the Fe^{3+}-chelated cellulose monolayer. Similarly, the binding energy of the Fe^{3+}-chelated hemicellulose monolayer (–738.6 kJ/mol, Fig. 8**b**) is more negative than that of the original hemicellulose monolayer (–92.0 kJ/mol), indicating the higher stability of Fe^{3+}-chelated hemicellulose strands upon water exposure. Therefore, the coordination interactions between metal ions and lignocellulose ensure tight bonds among lignocellulose nanofibrils, making them less susceptible to water molecule disruption and facilitating the development hydrophobicity and water resistance.

4. Conclusions

We report a facile approach for converting conventional hydrophilic, low-wet-strength lignocellulosic paper to hydrophobic and water-resistant paper with high wet strength by immersion into an aqueous metal ion solution. During this process, metal ions (i.e., Fe^{3+}, Al^{3+}, and Zr^{4+}) coordinate with pulp fibers' polar groups (i.e., OH, C═O, and COOH) of their "hairy" surface lignocellulosic nanofibrils forming water stable bonding networks. This induces nanofibril self-assembly and cross linking to form a more compact structure with fewer OHs accessible to water, decreasing the paper surface energy and increasing its hydrophobicity and water resistance. The resulting hydrophobic paper exhibits WCAs as high as 140°, good wet tensile strengths of up to 9.5 MPa, and low water absorbency of <10 g/m^2. These properties are comparable to synthetic polymer films. Only 0.4 wt% of Fe^{3+} or Zr^{4+} ions are needed to endow the conventional unsized kraft packaging paper with hydrophobic properties. This low metal content and the water-stable metal-lignocellulose coordination interactions cause negligible metal ion leaching from the hydrophobic paper during water washing. Moreover, the paper remains hydrophobic after long-term ambient storage conditions and solvent washings. Furthermore, hydrophobic paper is biodegradable. This MIM approach can also be used to modify pulp for preparing hydrophobic tableware. A simple and low-cost method that converts conventional hydrophilic lignocellulosic paper and pulp to water-resistant packaging paper and tableware has been developed.

Declaration of Competing Interest

The authors declare that they have no known competing financial interests or personal relationships that could have appeared to influence the work reported in this paper.

Data availability

Data will be made available on request.

Acknowledgments

Dr. X. Zhang acknowledges the support from Forest and Wildlife Research Center (FWRC) at Mississippi State University through the FWRC Undergraduate Research Scholars Program. Dr. X. Zhang also thanks Ms. Madeline Gnann's participation in some experiments.

Appendix A. Supplementary data

Supplementary data to this article can be found online at https://doi.org/10.1016/j.cej.2023.141596.

References

[1] M. MacLeod, H.P.H. Arp, M.B. Tekman, A. Jahnke, The global threat from plastic pollution, Science 373 (2021) 61–65, https://doi.org/10.1126/science.abg5433.
[2] C. Liu, P. Luan, Q. Li, Z. Cheng, X. Sun, D. Cao, H. Zhu, Biodegradable, hygienic, and compostable tableware from hybrid sugarcane and bamboo fibers as plastic alternative, Matter 3 (2020) 2066–2079, https://doi.org/10.1016/j.matt.2020.10.004.
[3] Q. Xia, C. Chen, Y. Yao, J. Li, S. He, Y. Zhou, T. Li, X. Pan, Y. Yao, L. Hu, A strong, biodegradable and recyclable lignocellulosic bioplastic, Nat. Sustain. 4 (2021) 627–635, https://doi.org/10.1038/s41893-021-00702-w.
[4] Z. Markevičiūtė, V. Varžinskas, Plant-origin feedstock applications in fully green food packaging: the potential for tree-free paper and plant-origin bio-plastics in the Baltic sea region, Sustainability 14 (2022) 7393, https://doi.org/10.3390/su14127393.
[5] C. Chen, Y. Kuang, S. Zhu, I. Burgert, T. Keplinger, A. Gong, T. Li, L. Berglund, S. J. Eichhorn, L. Hu, Structure–property–function relationships of natural and engineered wood, Nat. Rev. Mater. 5 (2020) 642–666, https://doi.org/10.1038/s41578-020-0195-z.
[6] M. Wohlert, T. Benselfelt, L. Wågberg, I. Furó, L.A. Berglund, J. Wohlert, Cellulose and the role of hydrogen bonds: not in charge of everything, Cellulose 29 (1) (2022) 1–23, https://doi.org/10.1007/s10570-021-04325-4.
[7] Q.Q. Wang, J.Y. Zhu, R. Gleisner, T.A. Kuster, U. Baxa, S.E. McNeil, Morphological development of cellulose fibrils of a bleached eucalyptus pulp by mechanical fibrillation, Cellulose 19 (2012) 1631–1643, https://doi.org/10.1007/s10570-012-9745-x.
[8] F. Serra-Parareda, Q. Tarrés, M.À. Pèlach, P. Mutjé, A. Balea, M.C. Monte, C. Negro, M. Delgado-Aguilar, Monitoring fibrillation in the mechanical production of lignocellulosic micro/nanofibers from bleached spruce thermomechanical pulp, Int. J. Biol. Macromol. 178 (2021) 354–362, https://doi.org/10.1016/j.ijbiomac.2021.02.187.
[9] V.A. Lovikka, P. Khanjani, S. Väisänen, T. Vuorinen, T.C. Maloney, Porosity of wood pulp fibers in the wet and highly open dry state, Microporous Mesoporous Mater. 234 (2016) 326–335, https://doi.org/10.1016/j.micromeso.2016.07.032.
[10] P. Samyn, Wetting and hydrophobic modification of cellulose surfaces for paper applications, J. Mater. Sci. 48 (2013) 6455–6498, https://doi.org/10.1007/s10853-013-7519-y.
[11] N. Asim, M. Badiei, M. Mohammad, Recent advances in cellulose-based hydrophobic food packaging, Emergent Mater. 5 (3) (2022) 703–718.
[12] G. Glenn, R. Shogren, X. Jin, W. Orts, W. Hart-Cooper, L. Olson, Per- and polyfluoroalkyl substances and their alternatives in paper food packaging, Compr. Rev. Food Sci. Food Saf. 20 (2021) 2596–2625, https://doi.org/10.1111/1541-4337.12726.
[13] Paper's resistance to wetting - A review of internal sizing chemicals and their effects, BioResources. 2 (2007) 106–145. doi: 10.15376/biores.2.1.106-145.
[14] J. Liu, C. Wang, C.M. Ewulonu, X. Chen, M. Wu, Y. Huang, Fabrication of superhydrophobic and degradable cellulose paper materials for straw application, Cellulose 29 (2022) 527–540, https://doi.org/10.1007/s10570-021-04279-7.
[15] L.A. Schaider, S.A. Balan, A. Blum, D.Q. Andrews, M.J. Strynar, M.E. Dickinson, D. M. Lunderberg, J.R. Lang, G.F. Peaslee, Fluorinated compounds in U.S. Fast food packaging, Environ. Sci. Technol. Lett. 4 (2017) 105–111, https://doi.org/10.1021/acs.estlett.6b00435.
[16] M.A. Hubbe, R.A. Gill, Fillers for papermaking: a review of their properties, usage practices, and their mechanistic role, BioResources 11 (2016) 2886–2963, https://doi.org/10.15376/biores.11.1.2886-2963.
[17] R. Ajdary, B.L. Tardy, B.D. Mattos, L. Bai, O.J. Rojas, Plant nanomaterials and inspiration from nature: water interactions and hierarchically structured hydrogels, Adv. Mater. 33 (28) (2021) 2001085, https://doi.org/10.1002/adma.202001085.
[18] X. Wang, Z. Pang, C. Chen, Q. Xia, Y. Zhou, S. Jing, R. Wang, U. Ray, W. Gan, C. Li, G. Chen, B. Foster, T. Li, L. Hu, All-natural, degradable, rolled-up straws based on cellulose micro- and nano-hybrid fibers, Adv. Funct. Mater. 30 (2020) 1910417, https://doi.org/10.1002/adfm.201910417.
[19] J.M.B. Fernandes Diniz, M.H. Gil, J.A.A.M. Castro, Hornification—its origin and interpretation in wood pulps, Wood Sci. Technol. 37 (2004) 489–494, https://doi.org/10.1007/s00226-003-0216-2.
[20] What happens to cellulosic fibers during papermaking and recycling? A review, BioResources. 2 (2007) 739–788. doi: 10.15376/biores.2.4.739-788.
[21] M. Shimizu, T. Saito, A. Isogai, Water-resistant and high oxygen-barrier nanocellulose films with interfibrillar cross-linkages formed through multivalent metal ions, J. Membr. Sci. 500 (2016) 1–7, https://doi.org/10.1016/j.memsci.2015.11.002.
[22] C. Chen, W. Sun, L. Wang, M. Tajvidi, J. Wang, D.J. Gardner, Transparent multifunctional cellulose nanocrystal films prepared using trivalent metal ion exchange for food packaging, ACS Sustain. Chem. Eng. 10 (2022) 9419–9430, https://doi.org/10.1021/acssuschemeng.2c01805.
[23] W. Yang, Y. Song, C. Li, H. Bian, H. Dai, C. Hu, Metal-coordination and surface adhesion-assisted molding enabled strong, water-resistant carboxymethyl cellulose films, Carbohydr. Polym. 298 (2022) 120084.
[24] Y. Zhang, Y. Qian, Y. Liu, C. Lei, G. Qiu, G. Chen, Multivalent metal ion cross-linked lignocellulosic nanopaper with excellent water resistance and optical performance, Biomacromolecules 23 (2022) 1920–1927, https://doi.org/10.1021/acs.biomac.1c01374.
[25] H. Dong, J.F. Snyder, K.S. Williams, J.W. Andzelm, Cation-induced hydrogels of cellulose nanofibrils with tunable moduli, Biomacromolecules 14 (2013) 3338–3345, https://doi.org/10.1021/bm400993f.
[26] T. Joffre, E.L.G. Wernersson, A. Miettinen, C.L. Luengo Hendriks, E.K. Gamstedt, Swelling of cellulose fibres in composite materials: constraint effects of the surrounding matrix, Compos. Sci. Technol. 74 (2013) 52–59, https://doi.org/10.1016/j.compscitech.2012.10.006.
[27] C. Fitz-Binder, T. Bechtold, Ca^{2+} sorption on regenerated cellulose fibres, Carbohydr. Polym. 90 (2012) 937–942, https://doi.org/10.1016/j.carbpol.2012.06.023.
[28] A. Kongdee, T. Bechtold, The complexation of Fe(III)-ions in cellulose fibres: a fundamental property, Carbohydr. Polym. 56 (2004) 47–53, https://doi.org/10.1016/j.carbpol.2003.12.001.
[29] A. Jaturapiree, A. Ehrhardt, S. Groner, H.B. Öztürk, B. Siroka, T. Bechtold, Treatment in swelling solutions modifying cellulose fiber reactivity – Part 1: accessibility and sorption, Macromol. Symp. 262 (2008) 39–49, https://doi.org/10.1002/masy.200850205.
[30] S. Hokkanen, A. Bhatnagar, M. Sillanpää, A review on modification methods to cellulose-based adsorbents to improve adsorption capacity, Water Res. 91 (2016) 156–173, https://doi.org/10.1016/j.watres.2016.01.008.
[31] Y. Ding, W. Xu, Y. Yu, H. Hou, Z. Zhu, One-step preparation of highly hydrophobic and oleophilic melamine sponges via metal-ion-induced wettability transition, ACS Appl. Mater. Interfaces 10 (2018) 6652–6660, https://doi.org/10.1021/acsami.7b13626.
[32] E. Khare, N. Holten-Andersen, M.J. Buehler, Transition-metal coordinate bonds for bioinspired macromolecules with tunable mechanical properties, Nat. Rev. Mater. 6 (2021) 421–436, https://doi.org/10.1038/s41578-020-00270-z.
[33] X. You, H. Wu, R. Zhang, Y. Su, L. Cao, Q. Yu, J. Yuan, K. Xiao, M. He, Z. Jiang, Metal-coordinated sub-10 nm membranes for water purification, Nat. Commun. 10 (2019) 4160, https://doi.org/10.1038/s41467-019-12100-0.
[34] K.-H. Choi, A.R. Kim, B.-U. Cho, Effects of alkali swelling and beating treatments on properties of Kraft pulp fibers, BioResources 11 (2016) 3769–3782, https://doi.org/10.15376/biores.11.2.3769-3782.
[35] S. Ghosh, A. Sharma, G. Talukder, Zirconium. An abnormal trace element in biology, Biol. Trace Elem. Res. 35 (1992) 247–271, https://doi.org/10.1007/BF02783770.
[36] P.T. Bhattacharya, S.R. Misra, M. Hussain, Nutritional aspects of essential trace elements in oral health and disease: an extensive review, Scientifica 2016 (2016) e5464373, https://doi.org/10.1155/2016/5464373.
[37] I. of Medicine, F. and N. Board, S.C. on the S.E. of D.R. Intakes, S. of I. and U. of D. R. Intakes, S. on U.R.L. of Nutrients, P. on Micronutrients, Dietary Reference Intakes for Vitamin A, Vitamin K, Arsenic, Boron, Chromium, Copper, Iodine, Iron, Manganese, Molybdenum, Nickel, Silicon, Vanadium, and Zinc, National Academies Press, 2002.
[38] S. Cheng, A. Huang, S. Wang, Q. Zhang, Effect of different heat treatment temperatures on the chemical composition and structure of Chinese fir wood, BioResources 11 (2016) 4006–4016, https://doi.org/10.15376/biores.11.2.4006-4016.
[39] M.i. Gao, Z. Jiang, W. Ding, B. Shi, Selective degradation of hemicellulose into oligosaccharides assisted by $ZrOCl_2$ and their potential application as a tanning agent, Green Chem. 24 (1) (2022) 375–383, https://doi.org/10.1039/D1GC03827C.
[40] X. Zhang, Q. Yan, J. Li, I.-W. Chu, H. Toghiani, Z. Cai, J. Zhang, Carbon-based nanomaterials from biopolymer lignin via catalytic thermal treatment at 700 to 1000 °C, Polymers 10 (2018) 183, https://doi.org/10.3390/polym10020183.
[41] Y. Ma, M. Hummel, M. Määttänen, A. Särkilahti, A. Harlin, H. Sixta, Upcycling of waste paper and cardboard to textiles, Green Chem. 18 (2016) 858–866, https://doi.org/10.1039/C5GC01679G.
[42] C.J. Biermann, Handbook of Pulping and Papermaking, 2nd edition, Academic Press, San Diego, 1996.
[43] R.P. Chandra, L.K. Lehtonen, A.J. Ragauskas, Modification of high lignin content Kraft pulps with laccase to improve paper strength properties. 1. Laccase treatment in the presence of Gallic acid, Biotechnol. Progress 20 (1) (2004) 255–261.
[44] X. Zhang, Q. Yan, W. Leng, J. Li, J. Zhang, Z. Cai, E.B. Hassan, Carbon nanostructure of Kraft lignin thermally treated at 500 to 1000 °C, Materials 10 (2017) 975, https://doi.org/10.3390/ma10080975.

[45] N.A. Fakhre, B.M. Ibrahim, The use of new chemically modified cellulose for heavy metal ion adsorption, J. Hazard. Mater. 343 (2018) 324–331, https://doi.org/10.1016/j.jhazmat.2017.08.043.
[46] J. Reyes-Rivera, T. Terrazas, Lignin Analysis by HPLC and FTIR, in: M. de Lucas, J. P. Etchhells (Eds.), Xylem Methods Protoc, Springer, New York, NY, 2017, pp. 193–211, https://doi.org/10.1007/978-1-4939-6722-3_14.
[47] T. Rashid, C.F. Kait, T. Murugesan, A "Fourier transformed infrared" compound study of lignin recovered from a formic acid process, Procedia Eng. 148 (2016) 1312–1319, https://doi.org/10.1016/j.proeng.2016.06.547.
[48] N.A. Zubir, C. Yacou, J. Motuzas, X. Zhang, J.C. Diniz da Costa, Structural and functional investigation of graphene oxide–Fe_3O_4 nanocomposites for the heterogeneous Fenton-like reaction, Sci. Rep. 4 (2014) 4594, https://doi.org/10.1038/srep04594.
[49] T. Han, Y. Wei, X. Jin, H. Jiu, L. Zhang, Y. Sun, J. Tian, R. Shang, D. Hang, R. Zhao, Hydrothermal self-assembly of α-Fe_2O_3 nanorings@graphene aerogel composites for enhanced Li storage performance, J. Mater. Sci. 54 (2019) 7119–7130, https://doi.org/10.1007/s10853-019-03371-5.
[50] Y. Wang, L. Li, P. Dai, L. Yan, L. Cao, X. Gu, X. Zhao, Missing-node directed synthesis of hierarchical pores on a zirconium metal–organic framework with tunable porosity and enhanced surface acidity via a microdroplet flow reaction, J. Mater. Chem. A. 5 (2017) 22372–22379, https://doi.org/10.1039/C7TA06060B.
[51] Y.I. Kim, W.E. Hatfield, Electrical, magnetic and spectroscopic properties of tetrathiafulvalene charge transfer compounds with iron, ruthenium, rhodium and iridium halides, Inorganica Chim. Acta 188 (1991) 15–24, https://doi.org/10.1016/S0020-1693(00)80911-1.
[52] C. Sleigh, A.P. Pijpers, A. Jaspers, B. Coussens, R.J. Meier, On the determination of atomic charge via ESCA including application to organometallics, J. Electron Spectrosc. Relat. Phenom. 77 (1996) 41–57, https://doi.org/10.1016/0368-2048(95)02392-5.
[53] H.R. Motamedian, A.E. Halilovic, A. Kulachenko, Mechanisms of strength and stiffness improvement of paper after PFI refining with a focus on the effect of fines, Cellulose 26 (2019) 4099–4124, https://doi.org/10.1007/s10570-019-02349-5.